Multicomponent Self-Assembly: Generation of Rigid-Rack Multimetallic Pseudorotaxanes

Hanadi Sleiman,[1a,b] Paul N. W. Baxter,[1b] Jean-Marie Lehn,*[,1b] Karri Airola,[1c] and Kari Rissanen[1c]

Department of Chemistry, American University of Beirut, Beirut, Lebanon, Institut LeBel, Université Louis Pasteur, 4 Rue Blaise Pascal, 67000 Strasbourg, France, and Department of Chemistry, University of Jyväskylä, Jyväskylä, Finland

Received February 26, 1997[⊗]

The rigid linear ligands **1a**−**g** and the macrocycle **2** undergo self-assembly via coordination with copper(I) ions to generate the series of rigid-rack inorganic pseudorotaxanes **3a**−**g**. These complexes have been characterized by analytical and spectroscopic methods. Their architecture has been confirmed by determination of the crystal structures of **3e**,**f**. The complex $[Cu_2(\mathbf{1e})(\mathbf{2})_2](PF_6)_2$ (**3e**) crystallizes in the space group *C*2/*c*, whereas complex $[Cu_2(\mathbf{1f})(\mathbf{2})_2](PF_6)_2$ (**3f**) gives crystals containing a single enantiomer in the chiral space group $P2_12_12_1$. The synthesis and solution structures of **3a**−**g** and the solid-state structures of **3e**,**f** are discussed in relation to the viability of multicomponent self-assembly as an approach to linear metal-ion arrays.

Introduction

Over the past few years, a more profound understanding of intermolecular interactions has enabled the design of increasingly complex molecular architectures in a single operation by the spontaneous assembly of a given set of components.[2−4] Self-assembly occurs in high yield and high specificity when the sought structure represents a thermodynamic minimum and may be generated through weak, reversible bonding events. In particular, inorganic self-assembly relies on the bringing together and organization of a set of ligands as directed by the electronic and geometrical preferences of the complexed metal ions.

We have been interested in applying this particularly attractive and economical construction strategy to generate supramolecular complexes displaying ordered arrays of metal ions such as helicates,[5−8] racks,[9,10] ladders,[11] cages,[12] and grid-type[13] complexes. Such structures may also find potential applications as functioning components within future molecular electronic devices. Materials composed of spatially well-defined linear arrays of metal ions, such as racks, are particularly interesting in that they may exhibit directional energy and electron transfer processes. In order to self-assemble a rack-type multimetallic complex, one needs to design the system such that only structures arising from the mutual recognition and binding of two different ligand entities on the metal ion are formed. Systems where the metal ion-directed self-assembly reaction brings together two identical ligand types, *i.e.* where "self-recognition" occurs, have been documented.[5] On the other hand, the self-organization of inorganic architectures comprising nonidentical ligands has been less frequently reported.[6,10,11,12] To generate rigid rack-type complexes comprising a linear array of metal ions, the present work explores the threading of macrocyclic ligands onto rigid-rod linear ligands as directed by tetrahedral metal ions. This multicomponent self-assembly process leads to a new class of multimetallic pseudorotaxane complexes.

The generation of rotaxanes and other interlaced molecules, such as catenanes and knots, has recently inspired the synthetic efforts of a number of laboratories.[14−16] In particular, the intriguing structure of these molecules, where the component parts are held together mechanically, has been put to use in the design of novel polymer materials as well as potential components of molecular machinery.[16−22] Early attempts at the generation of rotaxanes have focused on statistical, as well as covalent syntheses.[23−26] Recent developments in the field of

⊗ Abstract published in *Advance ACS Abstracts,* September 1, 1997.

(1) (a) American University of Beirut. (b) Université Louis Pasteur. (c) University of Jyväskylä.
(2) Lehn, J.-M. *Angew. Chem., Int. Ed. Engl.* **1990**, *29*, 1304; Lehn, J.-M. *Supramolecular Chemistry, Scope and Perspectives*; VCH: Weinheim, Germany, 1995; Chapter 9.
(3) Lindsey, J. S. *New J. Chem.* **1991**, *15*, 153. Whitesides, G. M.; Mathias, J. P.; Seto, C. T. *Science* **1991**, *254*, 1312.
(4) Philp, D.; Stoddart, J. F. *Angew. Chem*. **1996**, *108*, 1242; *Angew. Chem., Int. Ed. Engl*. **1996**, *35*, 1155, part 4.4.
(5) Constable, E. C. In *Comprehensive Supramolecular Chemistry*; Pergamon: Exeter, U.K., 1996; Vol. 9; pp 213−252.
(6) Hasenknopf, B.; Lehn, J.-M.; Fenske, D.; Baum, G. *Proc. Natl. Acad. Sci. U.S.A.* **1996**, *93*, 1397−1400.
(7) Hasenknopf, B.; Lehn, J.-M.; Kneisel, B. O.; Baum, G.; Fenske, D. *Angew. Chem.* **1996**, *108*, 1987−1990.
(8) Lehn, J.-M.; Rigault, A. *Angew. Chem., Int. Ed. Engl.* **1988**, *27*, 1095−1097.
(9) Hanan, G.; Arana, C.; Lehn, J.-M.; Fenske, D. *Angew. Chem., Int. Ed. Engl.* **1995**, 1122−1124.
(10) Sleiman, H.; Baxter, P. N. W.; Lehn, J.-M.; Rissanen, K. *J. Chem. Soc., Chem. Commun.* **1995**, 715−716.
(11) Baxter, P. N. W.; Hanan, G. S.; Lehn, J.-M. *J. Chem. Soc., Chem. Commun.* **1996**, 2019−2020
(12) Baxter, P. N. W.; Lehn, J.-M.; DeCian, A.; Fischer, J. *Angew. Chem., Int. Ed. Engl.* **1993**, *32*, 69−72.
(13) Baxter, P. N. W.; Lehn, J.-M.; Fischer, J.; Youinou, M.-T. *Angew. Chem., Int. Ed. Engl.* **1994**, *33*, 2284−2287.
(14) Schill, G. *Catenanes, Rotaxanes and Knots*; Academic: New York, 1971.
(15) Amabilino, D. B.; Raymo, F. M.; Stoddart, J. F. In *Comprehensive Supramolecular Chemistry*; Elsevier Science Ltd.: Amsterdam, 1996; Vol. 9, Chapter 4.
(16) Gibson, H. W.; Marand, H. *Adv. Mater.* **1993**, *5*, 11.
(17) Ballardini, R.; Balzani, V.; Credi, A.; Gandolfi, M. T.; Langford, S. J.; Menzer, S.; Prodi, L.; Stoddart, J. F.; Venturi, M.; Williams, D. J. *Angew. Chem., Int. Ed. Engl.* **1996**, *35*, 978−981.
(18) Benniston, A. C.; Harriman, A.; Lynch, V. M. *Tetrahedron Lett.* **1994**, *35*, 1473−1476.
(19) Benniston, A. C.; Harriman, A.; Lynch, V. M. *J. Am. Chem. Soc.* **1995**, *117*, 5275−5291.
(20) Bissell, R. A.; Cordova, E.; Kaifer, A. E.; Stoddart, J. F. *Nature (London)* **1994**, *369*, 133−137.
(21) Gibson, H. W.; Bheda, M. C.; Engen, P. T. *Prog. Polym. Sci.* **1994**, *19*, 843.
(22) Gibson, H. W.; Liu, S.; LeCavalier, P.; Wu, C.; Shen, Y. X. *J. Am. Chem. Soc.* **1995**, *117*, 852.
(23) Schill, G.; Zollenkopf, H. *Liebigs Ann. Chem.* **1969**, *721*, 53.
(24) Schill, G.; Henschel, R. *Liebigs Ann. Chem.* **1970**, *722*, 113.
(25) Schill, G.; Zurcher, C.; Vetter, W. *Ber. Dtsch. Chem. Ges.* **1973**, *106*, 228.

S0020-1669(97)00222-X CCC: $14.00

supramolecular chemistry have provided more viable synthetic routes to rotaxanes where the assembly of the linear component and the loop has been accomplished through a variety of intermolecular attractive forces. For example, a number of rotaxanes and polyrotaxanes have been synthesized by utilizing solvophobic interactions to thread cyclodextrin molecules on a variety of linear components.[27−29] The use of π-stacking attractive interactions has also led to the generation of a new class of pseudorotaxanes and rotaxanes,[15,30] including a series of photochemically and chemically controllable pseudorotaxane-like compounds.[17,31,32] Rotaxanes have also been constructed using hydrogen-bonding interactions.[33,34] Of particular interest to the present work is the utilization of metal-ion coordination to template the threading of the cyclic component onto the linear axle.[35] This procedure has been used for the construction of porphyrin-stoppered metallorotaxane systems that display extremely rapid rates of electron transfer between the two porphyrin units and may serve as models for the bacterial photosynthetic reaction centers.[36−38]

In the present work, this construction strategy has been applied to the generation of extended multinuclear systems of rotaxane type, with a rigid, well-defined spatial organization of their metal ions, rendering them suitable components of molecular devices. We thus report the high-yield self-assembly of a new class of rigid-rack multimetallic complexes **3a**−**g** displaying pseudorotaxane geometries. A preliminary report describing part of this work has recently appeared.[10]

Experimental Section

Materials and Methods. CH_2Cl_2 and CH_3CN were freshly distilled under argon from P_2O_5 and CaH_2, respectively. Macrocyclic component **2** was synthesized according to the literature procedure.[39] Oligobipyridine and pyridylpyridazine ligands **1a**−**g** were available from earlier work.[10−13] The ^{1}H NMR spectra of **3a**−**g** and ^{1}H−^{1}H COSY studies were carried out by Patrick Maltese on a Bruker AM 400 spectrometer. The ^{1}H NMR spectrum of **3g** was also recorded at 500 MHz and a complete assignment made in conjunction with ^{1}H−^{1}H COSY and NOESY measurements. Mass spectra were determined by FAB$^+$ using a ZAB-HF VG apparatus in a *m*-nitrobenzyl alcohol matrix, at the "Service de Spectrométrie de Masse", Université Louis Pasteur, Strasbourg, France. UV/vis spectra [λ_{max} in nm (ϵ in L·mol^{-1}·cm^{-1})] were measured on a Cary 3 spectrophotometer. Microanalyses were performed by the "Service Central d'Analyses du CNRS", Lyon, France, and the "Centre Régional de Microanalyse", Université Pierre et Marie Curie, Paris.

General Procedure for the Self-Assembly of Complexes 3a−f. To a suspension containing 1 molar equiv of **1a**−**f** and 2 molar equiv of macrocycle **2** in dichloromethane under an argon atmosphere, was added 1 equiv of $[Cu(CH_3CN)_4][PF_6]$ in acetonitrile (2 mL) via syringe. The dark-red-brown mixture was then stirred for 12 h at room temperature prior to workup.

$[Cu_2(1a)(2)_2][PF_6]_2$ (3a). **1a** (5.9 mg, 0.018 mmol), **2** (20.0 mg, 0.035 mmol), and $[Cu(CH_3CN)_4][PF_6]$ (13.1 mg, 0.035 mmol) were used in dichloromethane/acetonitrile (2 mL/2 mL). After solvent removal under reduced pressure, **3a** was isolated as a red solid in quantitative yield. It was crystallized by vapor diffusion of diehtyl ether into an acetone solution to yield dark-red crystals.

^{1}H NMR (δ ppm, relative to TMS, acetone-d_6, 25 °C): 2.81 (s, 6 H, H[**1a**-CH_3]; 3.50−3.98 (m, 40 H, H[**2**-CH_2)]; 6.36 (d, 8H, H[**2**-meta], J = 8.7 Hz); 7.41 (d, 2H, H[**1a**-5], J = 7.6 Hz); 7.61 (d, 8H, H[**2**-ortho], J = 8.7 Hz); 8.08 (t, 2H, H[**1a**-4], J = 7.8 Hz); 8.32 (d, 4H, H[**2**-3], J = 8.3 Hz); 8.36 (d, 2H, H[**1a**-3], J = 8.6 Hz); 8.38 (s, 4H, H[**2**-5]); 8.56 (m, 6H, H[**1a**-3′,4′,6′]); 8.97 (d, 4H, H[**2**-4], J = 8.3 Hz). FAB-MS (*m*/*z*, % relative intensity): 401.1 (19) (Cu·**1a**)$^+$; 567.3 (85) (**2**·H)$^+$; 629.2 (100) (Cu·**2**)$^+$; 799.2 (8.5) (**3a** − $2PF_6$)$^{2+}$; 967.4 (16) (**3a** − $2PF_6$ − Cu·**2**)$^+$; 1598.4 (4.3) (**3a** − $2PF_6$)$^+$; 1743.4 (8.5) (**3a** − PF_6)$^+$. UV/vis (λ_{max}, nm (ϵ, M^{-1} cm^{-1}), acetonitrile): 282 (8 × 10^4); 325 (9 × 10^4); 445 (6 × 10^3); 550 (3 × 10^3). Anal. Calc for $C_{90}H_{86}Cu_2F_{12}N_8O_{12}P_2.3H_2O$: C, 55.64; H, 4.77; N, 5.77. Found: C, 55.42; H, 4.88; N, 5.84.

$[Cu_2(1b)(2)_2][PF_6]_2$ (3b). **1b** (8.1 mg, 0.018 mmol), **2** (20.0 mg, 0.035 mmol), and $[Cu(CH_3CN)_4][PF_6]$ (13.1 mg, 0.035 mmol) were used in dichloromethane/acetonitrile (2 mL/2 mL). Complete dissolution of ligand **1b** occurred after 30 min, and the dark-brown mixture was stirred for 12 h at room temperature under argon. After solvent evaporation, the brown residue was chromatographed on a short silica column (1:1 acetone/dichloromethane). A dark red-brown fraction was collected and evaporated to yield **3b** (30.1 mg, 85%). Recrystallization by vapor diffusion of diethyl ether into a nitromethane solution yielded dark-red, X-ray-quality crystals of **3b**.

^{1}H NMR (δ ppm, relative to TMS, acetone-d_6, 25 °C): 3.52−4.20 (m, 40 H, H[**2**-CH_2); 6.41 (t, 4H, H[**1b**-meta], J = 7.4 Hz); 6.44 (d, 8H, H[**2**-meta], J = 8.6 Hz); 6.57 (t, 2H, H[**1b**-para], J = 7.4 Hz); 7.31 (d, 4H, H[**1b**-ortho], J = 7.1 Hz); 7.66 (d, 8H, H[**2**-ortho], J = 8.6 Hz); 7.69 (d, 2H, H[**1b**-5], J = 7.8 Hz); 8.15 (d, 4H, H[**2**-3], J = 8.4 Hz); 8.21 (t, 2H, H[**1b**-4], J = 7.8 Hz); 8.23 (s, 4H, H[**2**-5]); 8.38 (m, 4H, H[**1b**-3,3′]); 8.67 (br s, 4H, H[**1b**-4′,6′]); 8.80 (d, 4H, H[**2**-4], J = 8.4 Hz). FAB-MS (*m*/*z*, % relative intensity): 525.0 (21) (Cu·**1b**)$^+$; 629.2 (100) (Cu·**2**)$^+$; 861.2 (7.5) (**3b** − $2PF_6$)$^{2+}$; 1091.3 (13) (**3b** − $2PF_6$ − Cu·**2**)$^+$; 1722.4 (4.8) (**3b** − $2PF_6$)$^+$; 1867.3 (4.8) (**3b** − PF_6)$^+$. UV/vis (λ_{max}, nm (ϵ, M^{-1} cm^{-1}), acetonitrile): 278 (8 × 10^4); 328 (8 × 10^4); 437 (4 × 10^3); 549 (3 × 10^3).

$[Cu_2(1c)(2)_2][PF_6]_2$ (3c). **1c** (5.4 mg, 0.015 mmol), **2** (17.0 mg, 0.030 mmol), and $[Cu(CH_3CN)_4][PF_6]$ (11.2 mg, 0.030 mmol) were used in dichloromethane/acetonitrile (2 mL/2 mL). After solvent evaporation, the red-brown residue was chromatographed on a short silica column (2:1 acetone/dichloromethane). A dark red fraction was collected and evaporated. The residue was crystallized by vapor diffusion of diethyl ether into an acetone solution to yield dark-red needles of **3c** (20.0 mg, 70%).

^{1}H NMR (δ ppm, relative to TMS, acetone-d_6, 25 °C): 3.38−3.91 (m, 40 H, H[**2**-CH_2]); 3.94 (s, 6H, H[**1c**-CH_3]); 6.16 (d, 8H, H[**2**-meta], J = 8.0 Hz); 7.35 (d, 8H, H[**2**-ortho], J = 8.0 Hz); 7.47 (d, 2H, H[**1c**-5], J = 7.8 Hz); 7.62 (s, 2H, H[**1c**-5′]); 8.14 (t, 2H, H[**1c**-4], J = 7.8 Hz); 8.19 (d, 4H, H[**2**-3], J = 8.3 Hz); 8.29 (s, 4H, H[**2**-5]); 8.58 (d, 2H, H[**1c**-3], J = 7.8 Hz); 8.88 (d, 6H, H[**2**-4] and H[**1c**-2′],); 9.77 (d, 2H, H[**1c**-1′], J = 8.0 Hz). FAB-MS (*m*/*z*, % relative intensity): 425.1 (44) (Cu·**1c**)$^+$; 567.2 (16) (**2**·H)$^+$; 629.2 (100) (Cu·**2**)$^+$; 811.2 (7.8) (**3c** − $2PF_6$)$^{2+}$; 991.3 (16) (**3c** − $2PF_6$ − Cu·**2**)$^+$; 1622.4 (4.3) (**3c** − $2PF_6$)$^+$; 1767.3 (4.3) (**3c** − PF_6)$^+$. UV/vis (λ_{max}, nm (ϵ, M^{-1} cm^{-1}), acetonitrile): 280 (8 × 10^4); 324 (9 × 10^4); 449 (7 × 10^3); 565 (3 × 10^3). Anal. Calc for $C_{92}H_{86}Cu_2F_{12}N_8O_{12}P_2$: C, 57.77; H, 4.53; N, 5.86. Found: C, 57.63; H, 4.71; N, 5.72.

$[Cu_2(1d)(2)_2][PF_6]_2$ (3d). **1d** (6.4 mg, 0.013 mmol), **2** (15.0 mg, 0.026 mmol), and $[Cu(CH_3CN)_4][PF_6]$ (9.9 mg, 0.026 mmol) were used in dichloromethane/acetonitrile (2 mL/2 mL). After solvent evaporation, the red-brown residue was chromatographed on a short silica column (2:1 acetone/dichloromethane). A dark brown fraction was collected and evaporated to yield **3d** (25.0 mg, 94.5%) as a brown solid. Crystals of **3d** were grown by vapor diffusion of diethyl ether into an acetone solution.

(26) Schill, G.; Schweickert, N.; Fritz, H.; Vetter, W. *Angew. Chem., Int. Ed. Engl.* **1983**, *22*, 889.
(27) Ogino, H. *J. Am. Chem. Soc.* **1981**, *103*, 1303.
(28) Ogino, H.; Ohata, K. *Inorg. Chem.* **1984**, *23*, 3312.
(29) Ogino, H. *New J. Chem.* **1993**, *17*, 683.
(30) Amabilino, D. B.; Stoddart, J. F. *Chem. Rev.* **1995**, *95*, 2725−2828.
(31) Asakawa, M.; Iqbal, S.; Stoddart, J. F.; Tinker, N. D. *Angew. Chem., Int. Ed. Engl.* **1996**, *35*, 976.
(32) Ashton, P. R.; Iqbal, S.; Stoddart, J. F.; Tinker, N. *J. Chem. Soc., Chem. Commun.* **1996**, 479−481.
(33) Ashton, P. R.; Glink, P. T.; Stoddart, J. F.; Tasker, P. A.; White, A. J. P.; Williams, D. J. *Chem. Eur. J.* **1996**, *2*, 729−736.
(34) Asakawa, M.; Ashton, P. R.; Brown, G. R.; Hayes, W.; Menzer, S.; Stoddart, J. F.; White, A. J. P.; Williams, D. J. *Adv. Mater.* **1996**, *8*, 37.
(35) Sauvage, J.-P. *Acc. Chem. Res.* **1990**, *23*, 319.
(36) Chambron, J.-C.; Heitz, V.; Sauvage, J.-P. *J. Am. Chem. Soc.* **1993**, *115*, 12378.
(37) Chambron, J.-C.; Harriman, A.; Heitz, V.; Sauvage, J.-P. *J. Am. Chem. Soc.* **1993**, *115*, 6109.
(38) Chambron, J.-C.; Chardon-Noblat, S.; Harriman, A.; Heitz, V.; Sauvage, J.-P. *Pure Appl. Chem.* **1993**, *65*, 2343−2349.
(39) Dietrich-Buchecker, C. O.; Sauvage, J.-P. *Tetrahedron* **1990**, *46*, 503

^{1}H NMR (δ ppm, relative to TMS, acetone-d_6, 25 °C): 3.66−3.94 (m, 40 H, H[**2**-CH_2]); 6.09 (d, 8H, H[**2**-meta], J = 8.7 Hz); 6.23 (t, 4H, H[**1d**-meta], J = 7.7 Hz); 6.42 (t, 2H, H[**1d**-para], J = 7.7 Hz); 7.12 (d, 4H, H[**1d**-ortho], J = 8.4 Hz); 7.37 (d, 8H, H[**2**-ortho], J = 8.7 Hz); 7.63 (d, 2H, H[**1d**-5], J = 7.9 Hz); 7.83 (s, 2H, H[**1d**-5′]); 7.89 (d, 4H, H[**2**-3], J = 8.4 Hz); 7.97 (s, 4H, H[**2**-5]); 8.14 (t, 2H, H[**1d**-4], J = 7.9 Hz); 8.52 (d, 4H, H[**2**-4], J = 8.4 Hz); 8.55 (d, 2H, H[**1d**-3], J = 7.9 Hz); 8.94 (d, 2H, H[**1d**-2′], J = 8.8 Hz); 9.83 (d, 2H, H[**1d**-1′], J = 8.8 Hz). FAB-MS (*m*/*z*, % relative intensity): 629.2 (100) (Cu·**2**)$^+$; 873.3 (9.7) (**3d** − $2PF_6$)$^{2+}$; 1115.3 (14) (**3d** − $2PF_6$ − Cu·**2**)$^+$; 1622.4 (4.3) (**3c** − $2PF_6$)$^+$; 1767.3 (4.3) (**3c** − PF_6)$^+$. UV/vis (λ_{max}, nm (ϵ, M^{-1} cm^{-1}), acetonitrile): 279 (8×10^4); 332 (8×10^4); 412 (5×10^3); 570 (3×10^3). Anal. Calc for $C_{102}H_{90}Cu_2F_{12}N_8O_{12}P_2$: C, 60.15; H, 4.45; N, 5.50. Found: C, 60.16; H, 4.61; N, 5.21.

[Cu$_2$(1e)(2)$_2$][PF$_6$]$_2$ (3e). **1e** (3.59 mg, 0.013 mmol), **2** (15.0 mg, 0.026 mmol), and [Cu(CH_3CN)$_4$][PF_6] (9.9 mg, 0.026 mmol) were used in dichloromethane/acetonitrile (2 mL/2 mL). After solvent removal, **3e** was isolated as a red solid by slow diffusion of diethyl ether into an acetone solution (22 mg, 93%). Dark-red, X-ray-quality crystals of **3e** were obtained by slow diffusion of diisopropyl ether into an acetone solution.

^{1}H NMR (δ ppm, relative to TMS, acetone-d_6, 20 °C): 1.89 (s, 6H, H[**1e**-CH_3]); 3.72−4.00 (m, 40 H, H[**2**-CH_2]); 6.26 (d, 8H, H[**2**-meta], J = 8.8 Hz); 6.83 (d, 8H, H[**2**-ortho], J = 8.8 Hz); 7.58 (d, 2H, H[**1e**-5], J = 7.8 Hz); 7.82 (d, 4H, H[**2**-3], J = 8.4 Hz); 8.17 s, 4H, H[**2**-5]); 8.18 (t, 2H, H[**1e**-4], J = 8.1 Hz); 8.55 (d, 2H, H[**1e**-3], J = 7.8 Hz); 8.60 (d, 4H, H[**2**-4], J = 8.4 Hz); 9.13 (s, 2H, H[**1e**-3′]). FAB-MS (*m*/*z*, % relative intensity): 325.1 (21) (Cu·**1e**)$^+$; 629.2 (100) (Cu·**2**)$^+$; 761.2 (8.3) (**3e** − $2PF_6$)$^{2+}$; 891.3 (54) (**3e** − $2PF_6$ − Cu·**2**)$^+$; 1522.5 (8.3) (**3e** − $2PF_6$)$^+$; 1667.4 (8.3) (**3e** − PF_6)$^+$. UV/vis (λ_{max}, nm (ϵ, M^{-1} cm^{-1}), acetonitrile): 283 (9×10^4), 306 (7×10^4), 440 (6×10^3), 465 (7×10^3), 520 (5×10^3).

[Cu$_2$(1f)(2)$_2$][PF$_6$]$_2$ (3f). **1f** (5.02 mg, 0.013 mmol), **2** (15.0 mg, 0.026 mmol), and [Cu(CH_3CN)$_4$][PF_6] (9.9 mg, 0.026 mmol) were used in dichloromethane/acetonitrile (2 mL/2 mL). After solvent removal, **3f** was isolated as a dark-red solid by slow diffusion of diethyl ether into an acetone solution (20.5 mg, 85%). Dark-red, X-ray-quality crystals of **3f** were obtained by slow diffusion of diisopropyl ether into an acetone solution.

^{1}H NMR (δ ppm, relative to TMS, acetone-d_6, 25 °C): 3.63−3.99 (m, 40 H, H[**2**-CH_2]); 6.05 (t, 4H, H[**1f**-meta], J = 7.5 Hz); 6.24 (d, 8H, H[**2**-meta], J = 8.8 Hz); 6.32 (t, 2H, H[**1f**-para], J = 7.5 Hz); 6.78 (d, 8H, H[**2**-ortho], J = 8.8 Hz), 6.97 (d, 4H, H[**1f**-ortho], J = 7.2 Hz); 7.52 (d, 4H, H[**2**-3], J = 8.4 Hz); 7.73 (d, 2H, H[**1f**-3], J = 7.7 Hz); 7.89 (s, 4H, H[**2**-5]); 8.28 (d, 4H, H[**2**-4], J = 8.5 Hz); 8.28 (t, 2H, H[**1f**-4], J = 7.9 Hz); 8.67 (d, 2H, H[**1f**-5], J = 7.9 Hz); 9.26 (s, 2H, H[**1f**-3′]). FAB-MS (*m*/*z*, % relative intensity): 629.2 (100) (Cu·**2**)$^+$; 823.3 (6.2) (**3f** − $2PF_6$)$^{2+}$; 1015.4 (32) (**3f** − $2PF_6$ − Cu·**2**)$^+$; 1647.5 (79) (**3f** − $2PF_6$)$^+$; 1791.5 (22) (**3f** − PF_6)$^+$. UV/vis (λ_{max}, nm (ϵ, M^{-1} cm^{-1}), acetonitrile): 277 (9×10^4), 321 (8×10^4), 438 (5×10^3), 593 (2×10^3).

[Cu$_3$(1g)(2)$_3$][PF$_6$]$_3$ (3g). **1g** (5.8 mg, 0.012 mmol) was suspended in CH_2Cl_2 (2 mL) and ultrasonicated for 1 h. Macrocycle **2** (20.0 mg, 0.035 mmol) was added as a solid, and the suspension was degassed (three freeze−pump−thaw cycles). A solution of [Cu(CH_3CN)$_4$][PF_6] (13.1 mg, 0.035 mmol) in acetonitrile (5 mL) was added via syringe, under an argon atmosphere. The dark-brown suspension was heated to reflux under argon, and the reflux maintained for 48 h. The solvents were then evaporated and the brown residue dissolved in acetone (2 mL). Pure **3g** was obtained in 90% yield as a dark-red precipitate by vapor diffusion of diethyl ether into this acetone solution.

^{1}H NMR (δ ppm, acetone-d_6, relative to acetone-h_6, 500MHz, 25 °C): 2.01 (s, 6H, H[**1g**-Me]); 3.47−3.88 (m, 60 H, H[outer/inner **2**-CH_2]); 6.33 (d, 8H, H[outer **2**-meta], $J_{m,o}$ = 8.7 Hz); 6.35 (d, 4H, H[inner **2**-meta″], $J_{m'',o''}$ = 8.7 Hz); 7.38 (d, 2H, H[**1g**-5], $J_{5,4}$ (**1g**) = 7.6 Hz); 7.57 (d, 8H, H[outer **2**-ortho], $J_{o,m}$ = 6.8 Hz); 7.61 (d, 4H, H[inner **2**-ortho″], $J_{o'',m''}$ = 8.6 Hz); 8.04 (t, 2H, H[**1g**-4], $J_{4,3}$, $J_{4,5}$(**1g**) = 7.8 Hz); 8.27 (d, 4H, H[outer **2**-3], $J_{3,4}$(outer **2**) = 8.3 Hz); 8.28 (d, 2H, H[inner **2**-3″], $J_{3'',4''}$(inner **2**) = 8.3 Hz); 8.33 (d, 2H, H[**1g**-3], $J_{3,4}$(**1g**) = 6.8 Hz); 8.33 (s, 4H, H[outer **2**-5]); 8.36 (s, 2H, H[inner **2**-5″]); 8.51 (s, 2H), 8.52 (s, 2H), H[**1g**-3′,4′]; 8.55 (dd, 2H, H[**1g**-4″], $J_{4'',3''}$(**1g**) = 8.5 Hz, $J_{4'',6''}$(**1g**) = 2.2 Hz); 8.61 (d, 2H, H[**1g**-6′], $J_{6',4'}$(**1g**) = 0.6 Hz); 8.62 (d, 2H, H[**1g**-3″], $J_{3'',4''}$(**1g**) = 7.6 Hz); 8.70 (d, 2H, H[**1g**-6″], $J_{6'',4''}$(**1g**) = 1.7 Hz); 8.92 (d, 4H, H[outer **2**-4], $J_{4,3}$-(outer **2**) = 8.3 Hz); 8.93 (d, 2H, H[inner **2**-4″], $J_{4'',3''}$(inner **2**) = 8.3 Hz). ^{13}C NMR (δ ppm, acetone-d_6, relative to acetone-h_6, 125 MHz, 25 °C): 164.2, 160.5, 158.8, 157.7, 152.5, 151.5, 147.8, 147.4, 144.6, 139.3, 139.1, 138.9, 136.9, 134.7, 133.9, 133.7, 130.5, 130.4, 129.1, 127.5, 126.6, 125.8, 125.6, 123.9, 121.2, 114.5 (aromatic carbons), 71.4, 71.3, 71.3, 71.2, 70.1, 68.9 (CH_2), 25.2 (CH_3). FAB-MS (*m*/*z*, % relative intensity): 1123.2 (16) (**3g** − $3PF_6$ − 2Cu·**2**)$^+$; 1264.1 (7.8) (**3g** − $2PF_6$)$^{2+}$; 1752.8 (16) (**3g** − $3PF_6$ − Cu·**2**)$^+$; 1897.9 (16) (**3g** − $2PF_6$ − Cu·**2**)$^+$; 2382.7 (4.3) (**3g** − $3PF_6$)$^+$; 2528.0 (4.3) (**3g** − $2PF_6$)$^+$; 2673.2 (4.3) (**3g** − PF_6)$^+$. UV/vis (λ_{max}, nm (ϵ, M^{-1} cm^{-1}), dichloromethane): 281 (10.1×10^4); 337 (12.7×10^4); 438 (11.3×10^3); 497 sh (6.8×10^3), 557 (4.7×10^3). Anal. Calc for $C_{134}H_{126}Cu_3F_{18}N_{12}O_{18}P_3$: C, 57.11; H, 4.51; N, 5.96. Found: C, 57.29; H, 4.28; N, 5.81.

Table 1. Crystallographic Data for **3e**,**f**

	3e	**3f**
chem formula	$C_{42}H_{41}CuN_4O_6^+PF_6^-$	$C_{102}H_{94}Cu_2N_9O_{14}^{2+}(PF_6^-)_2$
fw	906.30	2086.88
temp (°C)	20(2)	20(2)
λ (Å)	0.701 73	0.701 73
space group	*C*2/*c*	$P2_12_12_1$
a (Å)	22.199(4)	13.199(2)
b (Å)	17.227(3)	25.264(1)
c (Å)	21.109(4)	31.072(4)
β (deg)	95.18(2)	90
V (Å^3)	8040(3)	10361(2)
Z	8	4
ρ_{calc} (g cm^{-1})	1.498	1.338
μ (mm^{-1})	0.665	0.527
T_{min}/T_{max}	0.7710/0.9999	no abs corr
R^a	0.0700	0.964
$R_w{}^b$	0.1624	0.1527
absolute struct param	0.02(3)	

^{a} $R = \sum||F_o^2| - |F_c^2||/\sum|F_o^2|$. ^{b} $R_w = [\sum w(F_o^2 - F_c^2)^2]/\sum[w(F_o^2)^2]^{0.5}$.

X-ray Crystal Structure Determination. The X-ray crystallographic data were collected on an Enraf-Nonius CAD4 diffractometer using graphite-monochromatized Mo Kα radiation and $2\theta/\omega$ scans up to a 46° 2θ angle. Some crystallographic details are listed in Table 1.

The structures were solved with direct methods using the SHELXS-86 program[51] and refined as F^2 with SHELXL-93 program.[52] Hydrogens were refined as riding on their parent atoms. Semiempirical absorption correction using ψ-scans was applied to **3e** but not for **3f**. The absolute conformation was determined for **3f**.

Results and Discussion

Design Principle. The linear arrangement of metal ions in the desired architectures was accomplished by the use of the rigid, rodlike polytopic ligands **1a**−**g** constructed from 2,2′-bipyridine (bpy) (**1a**,**b**,**g**), pyridine−phenanthroline (py−phen) (**1c**,**d**), and pyridine−pyridazine subunits (py−pz) (**1e**,**f**).[12,13] The self-assembly of the macrocyclic 1,10-phenanthroline **2**[39] and **1** by means of metal ions of tetrahedral geometry such as copper(I) generates complexes **3a**−**g** in high yields (Schemes 1−3). Macrocycle **2** was used instead of the acyclic analogue in order to prevent two such units from coordinating to the same copper center. In addition, it was thought that the pseudorotaxane geometry of the system may render the complexes less labile during later electrochemical experiments, as dissociation of the complex can only result from a dethreading motion of the macrocycle **2** parallel to the axle ligand **1**. The self-assembly of each of the complexes **3a**−**g** will be described in the next sections. They were formed in 70%−quantitative yields according to NMR data on the crude mixture as obtained.

Preparation and Characterization. (a) Complexes 3a,b,g (Scheme 1). When a mixture of quaterpyridine (qpy) ligands **1a** or **1b**, 2 equiv of macrocyclic ligand **2** and 2 equiv of Cu(CH_3CN)$_4PF_6$ in CH_2Cl_2/CH_3CN was reacted for 12 h at room

Scheme 1. Self-Assembly of the Rigid-Rack Pseudorotaxane Complexes **3a**,**b**,**g**

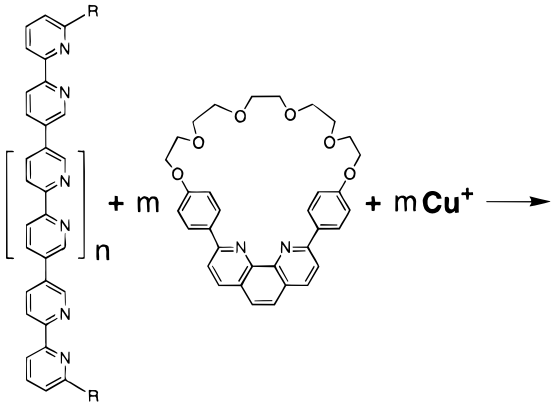

1a : n=0 R=Me **2**
1b : n=0 R=Ph
1g : n=1 R=Me

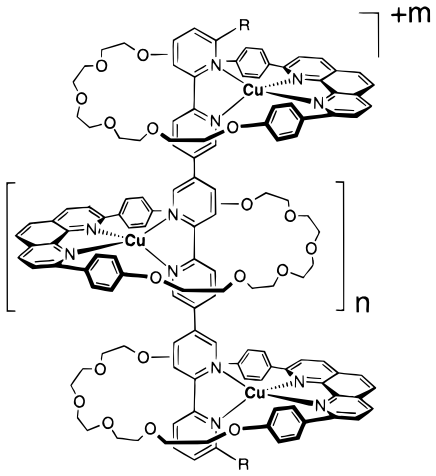

3a : n=0 m=2 R=Me
3b : n=0 m=2 R=Ph
3g : n=1 m=3 R=Me

temperature under argon, the spontaneous self-assembly of the dinuclear pseudorotaxane rack complexes **3a** and **3b** resulted. ^{1}H NMR of the mixture indicated that the copper(I)-directed self-assembly of quaterpyridine **1a** and macrocycle **2** had formed complex **3a** quantitatively, while complex **3b** formed in 90% yield according to the proton NMR spectrum. Complex **3a** was isolated quantitatively by solvent evaporation, and complex **3b** may be purified by column chromatography and was isolated in 85% yield. The pseudorotaxane rack **3g** also self-assembled in near quantitative yields, as judged by ^{1}H NMR, when sexipyridine ligand **1g** and 3 equiv macrocycle **2** were refluxed with 3 equiv $Cu(CH_3CN)_4PF_6$ for 48 h and was isolated (90%) by vapor diffusion of diethyl ether into an acetone solution.

Complexes **3a**,**b** result from the spontaneous and correct association of five particles (two phenanthrolines **2**, two copper(I) ions, and one qpy ligand **1a** or **1b**). In the case of complex **3g**, the mixture contains seven particles. It is interesting to note that mixing copper(I) ions with two different ligand types has lead to the exclusive self-assembly of heteroligand inorganic architectures. Mutual selection of two nonidentical ligand strands on the copper ion, rather than "self-recognition", has occured.

Scheme 2. Self-Assembly of the Rigid-Rack Pseudorotaxane Complexes **3c**,**d**

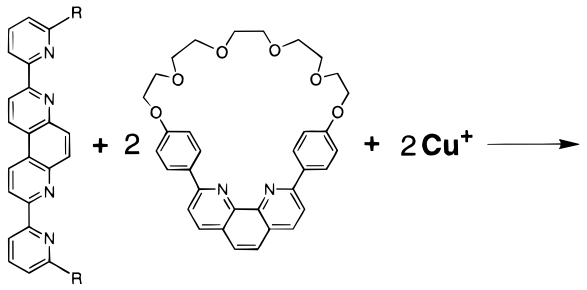

1c : R=Me **2**
1d : R=Ph

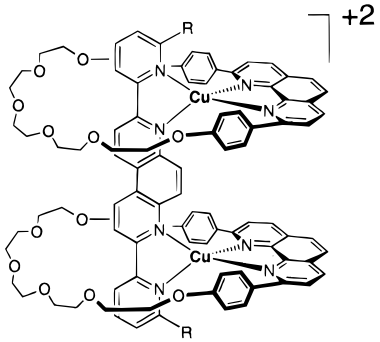

3c : R=Me
3d : R=Ph

Scheme 3. Self-Assembly of the Rigid-Rack Pseudorotaxane Complexes **3e**,**f**

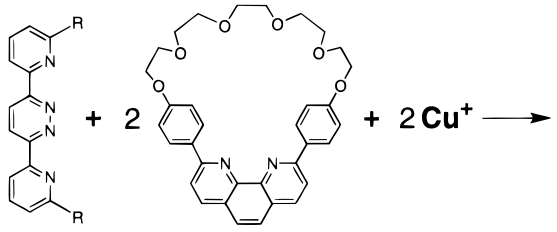

1e : R=Me **2**
1f : R=Ph

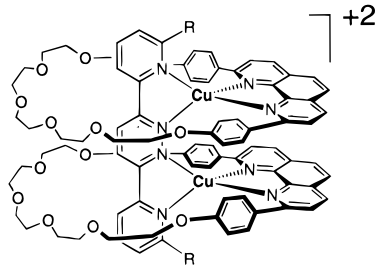

3e : R=Me
3f : R=Ph

The composition of complexes **3a**,**b**,**g** was confirmed by FAB-mass spectrometry. Figure 1 shows FAB-MS spectra for representative complexes **3a**,**c**,**e**,**g**. For all pseudorotaxane complexes generated in this work, the spectra show the successive loss of the PF_6^- counterions from the molecular ion. The peak clusters obtained for each fragment are in accordance with calculated ion intensities based on the isotopic distributions

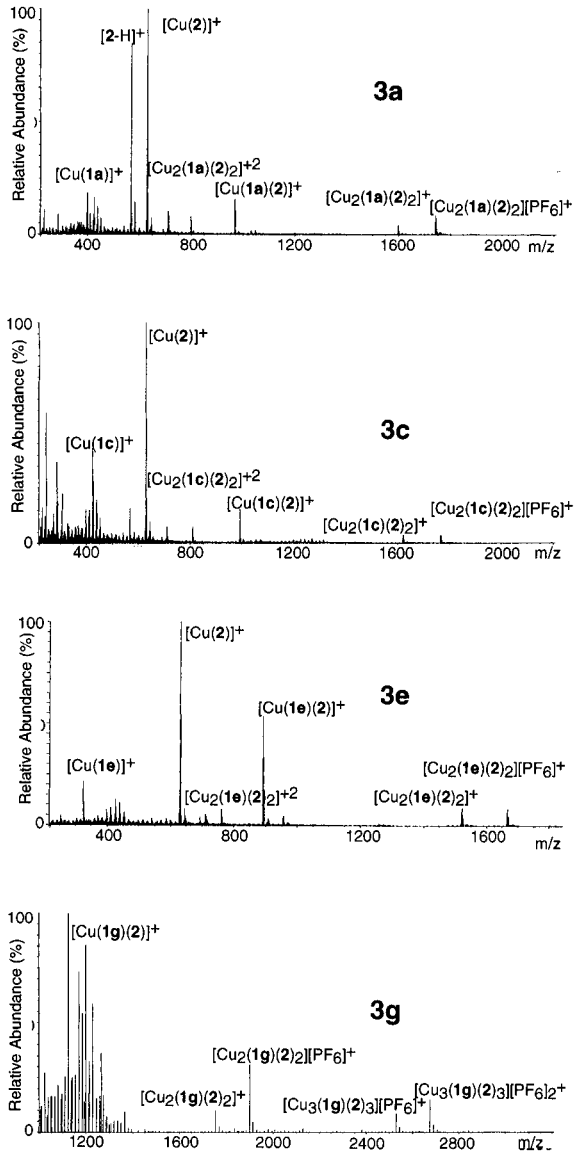

Figure 1. FAB-MS spectra of complexes **3a**,**c**,**e**,**g**.

for these fragments. The loss of PF_6^- ions is followed by dethreading the copper−(macrocycle **2**) moiety from the linear ligands **1a**,**b**,**g**. For complex **3g**, fragments arising from the dethreading of a first and a second copper−(macrocycle **2**) moiety are apparent. It is interesting to note that the dethreading of the pseudorotaxane complexes is the major mode of fragmentation in the FAB experiment; very little fragmentation of the ligands themselves was observed. In all dinuclear pseudorotaxanes, the copper−(macrocycle **2**) fragment was the base peak, in accordance with the relatively high stability of copper−phenanthroline complexes.

^{1}H NMR including ^{1}H−^{1}H COSY studies of complexes **3a**,**b**,**g** established that the threaded pseudorotaxane structure is stable in solution. The spectra show complexes comprised of macrocycle **2** and ligands **1** in a ratio of 2:1 in the cases of **3a**,**b** and 3:1 in the case of **3g**. The spectra are shown in Figure 2 for **3a**−**g**. The peaks corresponding to the phenyl rings of macrocycle **2** in the complexes **3a**−**g** all show a marked upfield shift (approximately 0.8 ppm) as compared to free macrocycle **2**. This is due to the exposure of these protons to the ring current of the 2,2′-bipyridyl subunits of ligand **1**. X-ray structure characterization of **3b** reveals in fact a $\pi-\pi$-stacking arrangement between these aromatic rings (*vide infra*). Similar effects have been observed in the characterization of metallocatenanes derived from the interlocking of two such macrocyclic ligands.[40] To a lesser extent, protons 4 and 5 on macrocycle **2** are moved downfield (approximately 0.5 ppm) upon complexation. All peaks corresponding to macrocycle **2** in diphenyl complex **3b** are slightly upfield of those in dimethyl complex **3a**.

When one compares the spectrum of **3a** to that of the uncomplexed ligand **1a**, an upfield shift of 0.6 ppm is noted for proton 6′. Similar effects have been found in complexes such as $Cu(bpy)_2^+$ and are due to the location of these protons in the ring current of the phen group of ligand **2**. It is somewhat surprising that protons 3 and 3′ do not shift noticeably upon complexation. The phenyl protons of ligand **1b** are considerably shifted upfield upon coordination (approximately 1.2 ppm) in complex **3b** and reflect the proximity of these rings to the phen rings of macrocycle unit **2**. X-ray analysis of complex **3b** (*vide infra*) is indeed indicative of a π-stacking interaction between these phenyl groups and the phen moieties of ligand **2**.

The structure of pseudorotaxane **3g** was assigned on the basis of ^{1}H−^{1}H COSY and NOESY measurements. All aromatic protons of the macrocycles **2** in complex **3g** are split into two groups of peaks in a ratio 2:1, corresponding respectively to the two outer and the one inner macrocycle **2** threading the sexipyridine ligand **3g**. The ^{1}H−^{1}H NOESY spectrum of **3g** shows through-space inter-ring H4′−H6″ and H6′−H4″ interactions within the central ligand **1g** which clearly demonstrate that **3g** exists in the sterically less congested transoid conformation in solution.

An X-ray structure analysis of complex **3b** showed it to display a high degree of spatial organization.[10] In **3b**, the whole qpy ligand is essentially planar with the two bpy subunits oriented in a transoid conformation. The phen subunit of each ligand **2** faces the pentaoxyethylene fragment of the other ligand **2** on the qpy backbone. In analogy to **3b**, it is expected that in the solid-state structures of the dinuclear and the trinuclear rotaxanes **3a**,**g**, the metal ions are consecutively located on opposite sides of the quater- and sexipyridine ligand backbone.

(b) Complexes 3c,d (Scheme 2). The copper(I)-directed threading of macrocycle **2** onto py−phen ligands **1c**,**d** is expected to yield the pseudorotaxane rack complexes **3c**,**d** where the metal ions are located on syn positions of ligands **1c**,**d**. This is in contrast to the anti arrangement found in complex **3b**. Complexes **3c**,**d** were generated in order to assess the effect of this cisoid arrangement on the structure and on the metal−metal electronic communication.

Thus, a mixture containing **1c** or **1d**, 2 equiv of macrocycle **2**, and 2 equiv of $Cu(CH_3CN)_4PF_6$ in CH_3CN/CH_2Cl_2 was stirred at room temperature under argon. After 12 h, the ^{1}H NMR showed **3c** to be the major product (85%). Heating the mixture in an attempt to complete the self-assembly process was not successful, and compound **3c** was isolated from the mixture by chromatography in 71% yield. **3d** on the other hand was formed nearly quantitatively after 12 h at room temperature and was isolated by chromatography in 95% yield.

Complexes **3c**,**d** showed FAB-mass spectra similar to those of **3a**,**b**,**g** (Figure 1). Successive loss of PF_6^- ions from the molecular ion is directly followed by dethreading of the copper−(macrocycle **2**) from the rigid linear ligands **1c**,**d**. Again, no other fragmentation is apparent in the FAB spectra, and the parent ion corresponds to Cu − $(\mathbf{2})^+$.

The ^{1}H NMR spectra (and ^{1}H−^{1}H COSY studies) of **3c**,**d** show upfield shifts of the phenyl peaks of macrocycle **2** upon complexation, similar to those observed for complexes **3a**,**b** (Figure 2). Going from the transoid conformation in **3a** to the cisoid conformation in **3c** (or from **3b** to **3d**) allows detection of a net upfield shift (approximately 0.3 ppm) of all the

(40) Dietrich-Buchecker, C. O.; Sauvage, J.-P.; Kintzinger, J.-P. *Tetrahedron Lett.* **1983**, *46*, 5095.

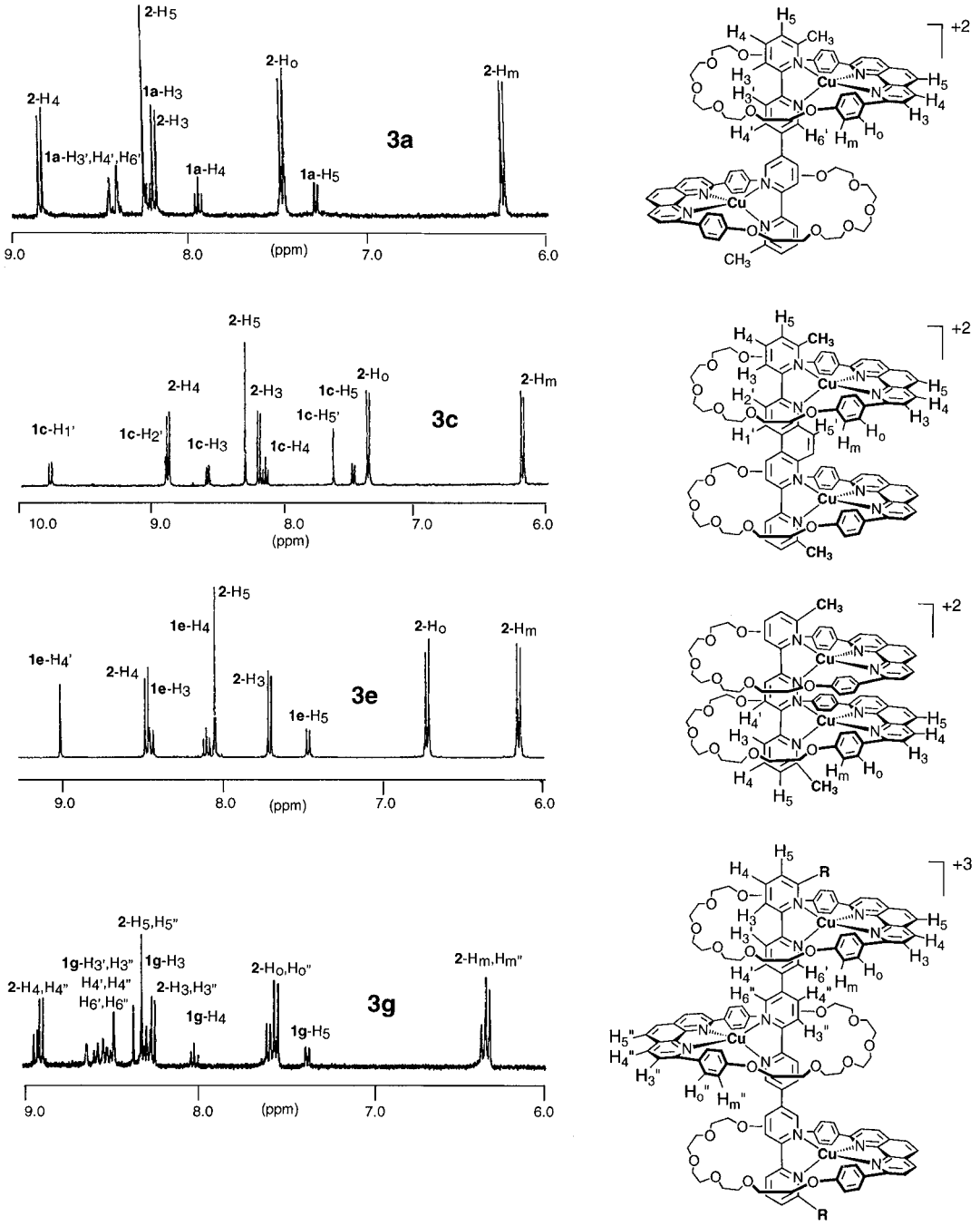

Figure 2. 400 MHz ^{1}H NMR spectra of complexes **3a**,**c**,**e**,**g** in acetone-d_6.

macrocycle **2** protons. This may reflect aromatic interactions due to the face-to-face arrangement of the phenanthroline moieties of ligands **2** in complexes **3c**,**d**. As was the case for complexes **3a**,**b**, peaks corresponding to macrocycle **2** in the diphenyl complex **3d** are shifted slightly upfield compared to those for ligand **2** in dimethyl complex **3c**.

When the spectra of **3c**,**d** are compared to those of uncomplexed ligands **1c**,**d**, a large upfield shift of proton 5′ (0.7 ppm) as well as a downfield shift of proton 2′ is detected; in **3c**,**d** proton 5′ points into the ring current of the phen subunit of ligand **2** while proton 2′ may point into the deshielding oxyethylene group. As in **3b**, the phenyl protons of ligand **1d** display large upfield shifts (approximately 1.1 ppm) upon formation of complex **3d**; the phenyl substituents of ligand **1d** are in proximity to the phenanthroline subunit of ligand **2**, and π-stacking interactions, in analogy to **3b**, may be present.

(c) Complexes 3e,f (Scheme 3). The self-assembly of copper(I) ions, macrocycle **2**, and py−pz ligand **1e** or **1f** is expected to yield the dinuclear pseudorotaxane rack complexes **3e**,**f** with a cisoid arrangement of the metal−phen moieties on the backbone of the linear ligands. In addition, the metal centers are in closer proximity than in complexes **3a**−**d** due to coordination to the same pyridazine ring. This spatial proximity is expected to significantly alter the structural and electrochemical properties of these complexes **3e**,**f**, relative to **3a**−**d** and **3g**. On the other hand, the close proximity of the phenyl subunits of ligands **2** may be expected to destabilize complexes **3e**,**f** and reduce the efficiency of the self-assembly process.

Addition to the py−pz ligand **1e** or **1f** of 2 equiv of macrocycle **2** and 2 equiv of $[Cu(CH_3CN)_4][PF_6]$ in CH_3CN/CH_2Cl_2 under argon, stirring at ambient temperature for 12 h, and subsequent workup yielded **3e**,**f** in 93% and 85% yields, respectively. Structural confirmation for complexes **3e**,**f** was accomplished using FAB-mass spectrometry (Figure 1). The spectra are quite similar to those of the previously described complexes in that initial successive PF_6^- counterions loss is followed by dethreading of the copper−(macrocycle **2**) moiety from the rigid-rod ligands **1**.

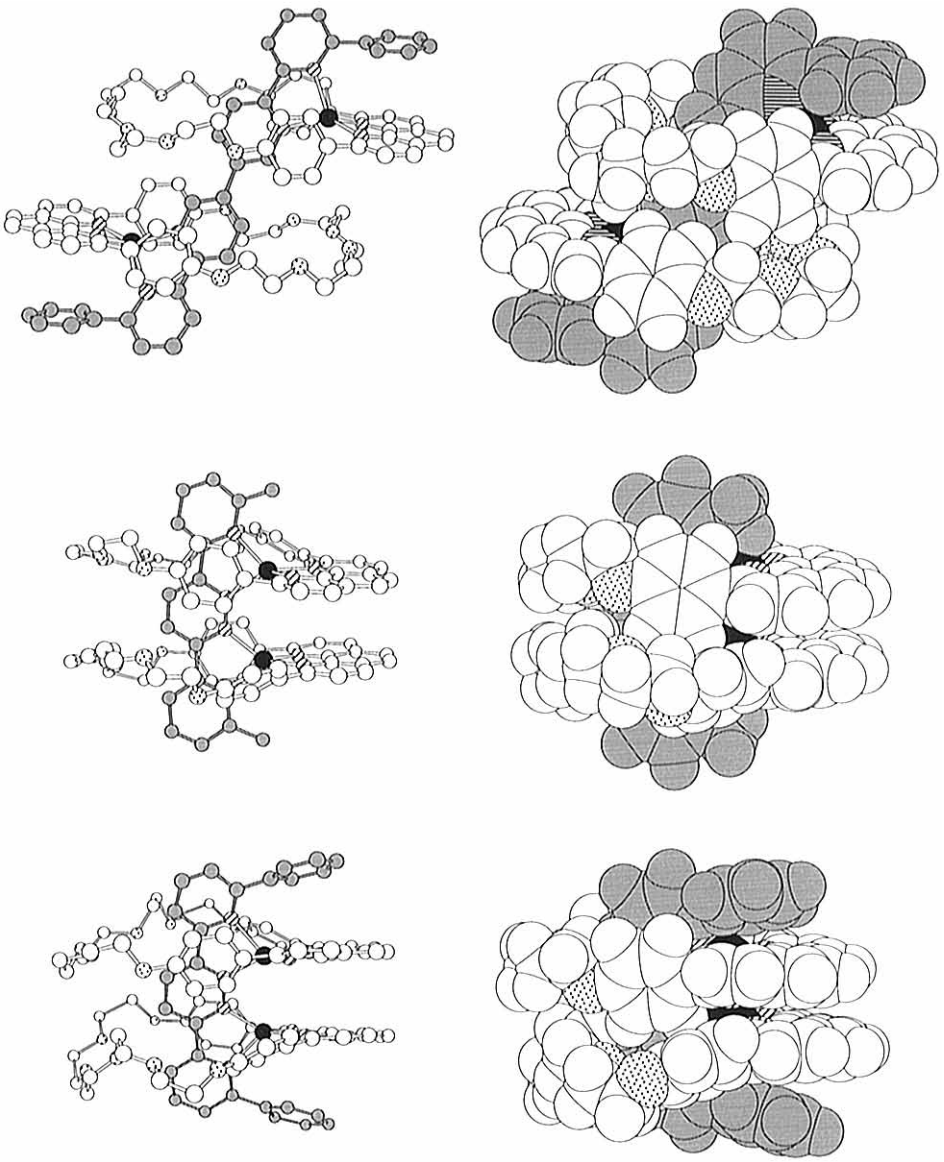

Figure 3. Crystal structures of the self-assembled dinuclear pseudorotaxane racks **3b**, $[Cu_2(\mathbf{1b})(\mathbf{2})_2](PF_6)_2$[10] (top), **3e**, $[Cu_2(\mathbf{1e})(\mathbf{2})_2](PF_6)_2$ (center), and **3f**, $[Cu_2(\mathbf{1f})(\mathbf{2})_2](PF_6)_2$ (bottom), showing ball and stick (left; hydrogen atoms omitted for clarity) and space-filling (right) representations.

The ^{1}H NMR studies of **3e**,**f** further establish the structure and the correct stoichiometry (1:2 for ligand **1e** or **1f**:**2**) for these complexes (Figure 2). It has been shown above that the macrocycle **2** protons are systematically shifted upfield on going from the transoid form (*e.g.* **3a**) to the cisoid form (*e.g.* **3c**). With the exception of the meta position, the protons of macrocycle **2** are moved further upfield by bringing the two copper−(phen **2**) centers closer together in complexes **3e**−**f**. The protons of macrocycle **2** displaying the greatest displacement upon threading are the ortho (0.8 ppm for **3e** compared to **3a**) and the 3-position (0.5 ppm for **3e** compared to **3a**). The large upfield shift of the ortho protons and, to a lesser extent, the 3-protons of the ligand **2** in complexes **3e**,**f** can be understood upon inspection of the X-ray crystal structures of **3e**,**f** (see below).

Upon complexation, the signals of the 3-protons of ligands **1e** (or **1f**) in **3e** or **3f** move noticeably downfield (0.4 ppm for **3e**). This is consistent with the fact that these protons point into and are deshielded by the oxyethylene chains of macrocycles **2**. As in the diphenyl pseudorotaxanes **3b**,**d**, the phenyl groups of ligand **1f** in complex **3f** are shifted significantly upfield upon coordination. This substantiates the π-stacking proximity of these phenyl rings to the phen subunits of ligand **2** (see structure of **3f** below).

X-ray Crystallographic Characterization of Complexes 3e,f (Table 1, Figure 3). Structure determination of the bimetallic pseudorotaxane complex **3b** established the high degree of spatial organization in such complexes.[10] The metal ion−(phen **2**) units are arranged in an anti conformation with respect to the qpy **1b** backbone. We were interested in the structural effects of constraining the metal ion−(phen **2**) racks to a syn conformation and the concomitant contraction of the copper ion separation. X-ray structure determinations were therefore carried out on complexes **3e**,**f**, which established the rigid-rack arrangement and the [3]-rotaxane topology in these complexes.

(a) Structure of $[Cu_2(\mathbf{1e})(\mathbf{2})_2][PF_6]_2$ (3e). X-ray-quality crystals of **3e** were grown by slow diffusion of diisopropyl ether into an acetone solution. The structure confirms that two macrocycles **2** are threaded on the rigid backbone of the py−pz ligand **1e** in a syn geometry. The Cu−Cu distance (3.69 Å) of **3e** represents a considerable reduction in metal ion separation compared to **3b** (9.86 Å). This contraction is greater than expected and results from the fact that the Cu^+ ions are not positioned centrally within the bidentate sites of **1e** but lie closer to the pyridazine ring nitrogens than to those of the outer pyridine rings. The two parallel oriented phen subunits of each ligand **2** are separated by 3.7 Å, which is suggestive of a weak

π-stacking interaction. It is interesting to note that these phen subunits are not eclipsed but display a substantial twist relative to one another (24°). This twist results from the close spatial arrangement of the copper−phen moieties and may somewhat relieve the steric interactions between the spatially confined phenyl groups of ligands **2** in the structure of **3e**. The cisoid conformation and the close proximity of the copper−phen units (3.69 Å) confines the two phenyl groups on each **2** ligand to a restricted space such that they are unable to both adopt an arrangement parallel to ligand **1e**. One ring of each **2** ligand is oriented parallel to the plane of **1e** (defined as ring 1; angle between rings = 10°) and is in a π-stacking interaction with this aromatic system (3.4 Å), while the other (ring-II) is tilted toward this plane. Additionally, two inter-**2** edge-to-face interactions occur between an ortho proton of each ring-I and ring-II of each partner **2** ligand (H(ring I)−center of ring-II = 2.7 Å), while an ortho proton of each ring-II is in contact with a pyridazine nitrogen of ligand **1e** (H−pdz N = 2.49 Å). This effect appears to persist in solution, as shown by the ^{1}H NMR of **3e** in which the ortho phenyl protons of ligands **2** are substantially shifted upfield as a result of lying within the ring current of **1e**. The presence of a single resonance due the ortho protons of **2** in the NMR spectrum of **3e** indicates that the two phenyl rings undergo fast interconversion on the NMR time scale. The molecule possesses a C_2 axis bisecting the pyridazine ring of ligand **1e**. The approximate plane of ligand **1e** is at an angle of 78° instead of 90° from the plane of the phen subunits of ligand **2** as a result of a distortion of the copper centers from tetrahedral geometry. In the dinuclear pseudorotaxane rack **3b**, this distortion is more pronounced and the angle is approximately 60°. In the latter structure, where the phen subunits are less constrained spatially, this distortion brings each of the outer pyridyl rings of ligand **1b** into π-stacking contact (3.4 Å) with one of the phenyl groups attached to the phen subunits of **2** and each of the inner pyridyl rings of **1b** in another π-stacking arrangement (3.4 Å) with the other phenyl groups on the phen subunits of **2**.

(b) Structure of $[Cu_2(1f)(2)_2][PF_6]_2$ (3f). Dark-red, X-ray-quality crystals of complex **3f** were obtained by slow diffusion of toluene into a nitromethane solution. The two threaded macrocyclic units **2** are in a cisoid arrangement on the rigid backbone of ligand **1f**. This complex exhibits a Cu−Cu separation of 3.52 Å, which is even shorter than that of **3e** (3.69 Å) and probably results from additional inward steric compression by the phenyl rings of **1f**. A weak inter-phenanthroline π-stacking interaction exists between the phenanthroline subunits of ligands **2**, which are oriented in parallel planes (distance 3.5 Å) and twisted from an eclipsed arrangement as in structure **3e**, by an angle of 42°. The absence of a C_2 axis bisecting the pz ring in **3f** is noteworthy. The coordination environments around each copper center, as well as the geometry of the two phenanthroline/py−pz binding sites are different for this complex. The phenyl groups on the 6-positions of the py units of ligand **1f** are oriented in a near face-to-face arrangement with the phen subunits and at a distance of 3.6 Å (3.9 Å for the second coordination site) suggestive of another set of weak π-stacked interactions in complex **3f**. The spatial confinement of the phenyl groups of ligands **2** results in an arrangement similar to that of complex **3e**. Ring-I is nearly parallel to the plane of **1f** and at a distance of closest contact of 3.2 Å (3.2 Å) from the pz ring of **1f**, and ring-II is tilted toward this plane. The edge-to-face interactions of the ortho hydrogens are 2.4 Å (2.6 Å) for the hydrogens of ring-I and 2.7 Å (2.7 Å) for ring-II. In solution, the phenyl rings on ligand **2** are in fast interconversion on the ^{1}H NMR time scale, as evidenced by the single resonance for these hydrogens in the spectrum of **3f**.

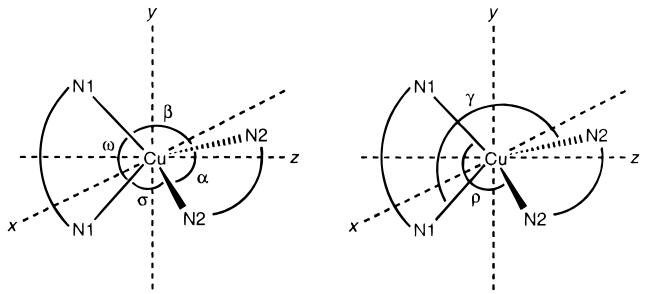

Figure 4. Schematic representation of intra- and interligand angles, where N1−N1 are the chelating nitrogens of ligands **1b**,**e**,**f** and N2−N2 are those of the macrocycle **2** ligands.

Table 2. Angular Distortions (θ) of the Cu(I) Centers from Tetrahedral Geometry and Intraligand (N1−Cu−N1, N2−Cu−N2) and Interligand (N1−Cu−N2) Angles for Complexes **3b**,**e**,**f**

	angles (deg)								
	θ_x	θ_y	θ_z	α	ω	β	σ	γ	ρ
$[Cu(dmp)_4]ClO_4$	92.8	83.2	98.2	81.3	81.7	126.9	130.8	114.9	127.0
3b	92.9	113.1	93.5	83.8	86.6	130.2	106.9	122.7	103.7
3e	84.2	77.8	96.9	82.5	80.7	118.4	139.3	115.2	124.7
3f	76.6	77.0	76.5	82.6	80.3	102.7	135.5	129.8	127
3f′	99.7	99.2	73.4	85.2	80.9	127.7	104.4	130	132.4

A pseudo-C_2 axis bisecting the pz ring of ligand **1f** is observed in the structure of **3f**. The approximate plane of ligand **1f** is at a dihedral angle of 68° instead of 90° from the plane of the phenanthroline subunits of ligand **2** as a result of a distortion of the copper centers from tetrahedral geometry. In both complexes **3e**,**f**, the py−pz ligands are slightly curved due to the fact that the pyridazyl ring is not a regular hexagon but is slightly contracted along the shorter N═N bond.

(c) Distortion of the Copper(I) Centers from Ideal Tetrahedral Geometry. It is interesting to examine the distortion of the copper(I) centers from ideal tetrahedral geometry in greater detail, as it arises both from the accommodation of the steric demands of the system and the maximization of weak attractive forces. In this respect, angular distortions such as the ones defined for the reference complex copper(I) bis(2,9-dimethyl-1,10-phenanthroline) $[Cu(dmp)_2^+]$ are pertinent.[41] If one places the copper(I)−phen **2** unit in the *xz* plane, with the *z* axis bisecting the N2−Cu−N2 angle, then a distortion θ_z is defined by the twist of the plane of N1−Cu−N1 around the *z*-axis (Figure 4). Similarly, θ_x and θ_y are defined by the twist of the N1−Cu−N1 plane relative to the Cu−phen plane around the *x*- and the *y*-axes, respectively. For an ideal tetrahedral ion, $\theta_x = \theta_y = \theta_z = 90°$. Table 2 lists these values for complexes **3b**,**e**,**f** as well as for the reference complex.[41] Keeping in mind that crystal packing forces as well as bite angles of the bidentate nitrogen ligand subunits (Table 2, Figure 4) can cause significant deviations of these angles, as illustrated by $Cu(dmp)_2^+$, complexes **3e**,**f** exhibit significant distortions from an ideal tetrahedral geometry. Rotations of the N1−Cu−N1 unit around the *x*, *y*, and *z* axes enhance the efficiency of nonbonded interactions in these complexes. A twist of ligand **1e**,**f** around the defined *z*-axis (θ_z) brings the phenyl rings on the phen subunits of **2** in close proximity to the aromatic rings of ligands **1**, thus allowing a more efficient $\pi-\pi$-stacking interaction. This twist results in a deviation of the dihedral angle between the planes of ligands **1** and **2** from the ideal value of 90°, as reported before. In addition, a twist of each of the bidentate subunits of ligands **1e** or **1f** around the *y*-axis (θ_y) allows a closer approach of the aromatic rings of these ligands to the parallel phenyl ring on the phen subunits of **2** (ring-I).

(41) Dobson, J.; Green, B. E.; Healy, P. C.; Kennard, C.; Pakawatchai, C.; White, A. H. *Aust. J. Chem.* **1984**, *37*, 649−659.

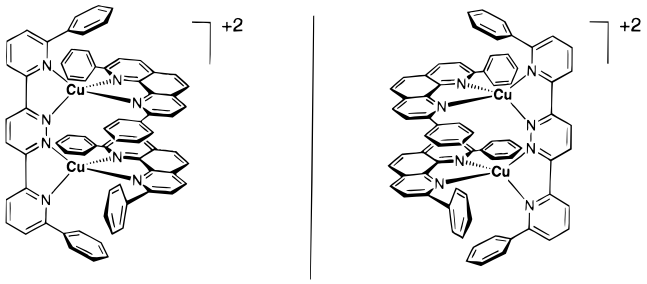

Figure 5. Schematic representation of the conformational enantiomers of complex **3f** (oxoethylene bridges omitted for clarity).

This rotation may also relieve the steric interactions between the phenyl groups residing on the spatially confined phen subunits of ligands **2**. It results in the previously reported deviation of the parallel phen subunits from a fully eclipsed cisoid arrangement. Finally, a twist of ligand **1f** around the *x*-axis brings the phenyl groups on the 6-positions in closer π-stacked proximity to the phen units of ligand **2**. Thus, the copper(I) centers are distorted from an ideal tetrahedral geometry to allow an arrangement of the ligands that minimizes steric interactions and maximizes $\pi-\pi$-stacking. In structure **3b**, a further distortion occurs in the form of a substantial displacement of the copper ion outside the approximate plane of the qpy ligand **1b** (17°).

(d) Enantiomorphism in the Crystal Structure of 3f. It is interesting to note that complex **3f** crystallizes in a chiral space group (orthorhombic, $P2_12_12_1$). This indicates that, in the crystal, the molecules **3f** are chiral. Indeed, when considering the solid-state structure of **3f**, it is noted that (i) the phenyl groups on the phenanthroline ligands **2** are not both parallel to ligand **1f** and (ii) the phenyl groups of ligand **1f** are rigidly oriented parallel to the phenanthroline subunits of **2**. These two facts make molecule **3f** non-superimposable on its mirror image (Figure 5). However, the barrier to rotation of the phenyl rings on ligand **2** is expected to be low. Thus, the conformational enantiomers shown in Figure 5 interconvert in solution as shown by the single resonance observed for all ortho protons (and all meta protons) on these rings. In the crystal, the molecular conformation is frozen. The chiral space group of the crystal of **3f** indicates that all molecules in this crystal are those of exclusively one enantiomer; thus, spontaneous resolution has taken place during the crystallization of complex **3f**. This process does not take place in the case of **3e**, which should display similar asymmetry in its solid-state structure. Complex **3e** crystallizes in the *C*2/*c* space group which possesses a plane of symmetry; the unit cell of crystals of **3e** contain both enantiomers of this complex. In the crystal lattice of **3f**, each pair of pseudorotaxane molecules orient their tail-ends toward each other, in such a way that the phenanthroline subunits of one molecule are in the same direction as the oxyethylene chains of the other. One toluene molecule of crystallization is encapsulated in the cavity defined by these tail-ends and may play an important role in the spontaneous resolution of complex **3f**. Thus when the first molecule of toluene is captured in the niche of ligands **1f** and **2**, the direction of axial twisting of ligand **1f** and thus the handedness of the entire molecule **3f** is chosen. The second **3f** molecule that closes the toluene into the cavity is of the same handedness as the first pseudorotaxane. This selection of handedness is then followed throughout the entire crystallization process. Resolutions through crystallization have been observed for a number of systems where the enantiomers are in equilibrium in the crystallization experiment.[42−47] For some systems where racemization is rapid, crystallizations leading to optically active crystals have been reported.[48−50] It is not clear to us whether the spontaneous resolution of complex **3f** has resulted in any enantiomeric excess. It is however interesting that the placement of the two phenanthroline subunits of ligands **2** in a syn fashion and in close proximity in complex **3f** has resulted in conformational chirality and the clathrate-type inclusion of a toluene molecule has led to selective recognition of the conformational enantiomers during the crystallization process, leading to homochiral crystals.

Conclusion

We have generated a new class of multimetallic pseudorotaxane rack complexes that display well-defined, rigid architectures and a linear arrangement of metal centers. In addition to the potential applications that these complexes may find as components of molecular electronic devices, the construction process is an example of an inorganic multicomponent self-assembly, where two different ligand types are brought together as directed by metal ions to form the final supramolecular species. The generality of this construction principle has been established. Such one-dimensional ordered arrays of metal complexes may be generated using a variety of rigid-rod, polytopic ligands. Therefore, the factors that play a role in the utilization of these self-assembled complexes as components of molecular devices, such as the distance between metal centers, as well as the amount of metal−metal interaction can be modulated with little alteration in the efficiency of the construction process, as demonstrated by the generation of complexes **3e**,**f**. The stability of these complexes stems from (i) the significant amount of encapsulation of the copper ions, (ii) the mechanical hindrance of the dethreading process which requires a motion of the macrocyclic ligand **2** parallel to the ligands **1** on the complex, and (iii) a large number of noncovalent interactions such as $\pi-\pi$ stacking and aromatic edge-to-face interactions, largely afforded by subtle distortions of the copper-(I) ions from an ideal tetrahedral geometry.

Future efforts will include the systematic study of electron transfer processes between the metal ions in these multimetallic complexes and assessment of their usefulness as rigid components of molecular electronic devices.

Acknowledgment. We thank the CNRS (URA 422) for financial support and a postdoctoral fellowship to H.S. and the Collège de France for a postdoctoral fellowship to P.N.W.B.

Supporting Information Available: X-ray crystallographic files, in CIF format, for the structures of complexes **3e**,**f** are available on the Internet only. Access information is given on any current masthead page.

IC9702227

(42) Abrahams, S. C.; Collin, R. L.; Lipscomb, W. N. *Acta Crystallogr.* **1951**, *4*, 15−20.
(43) Bois, C. *Acta Crystallogr.* **1972**, *B28*, 25−31.
(44) Brown, C. J.; Sadanaga, R. *Acta Crystallogr.* **1965**, *18*, 158−164.
(45) Herbstein, F. H.; Schmidt, G. M. J. *J. Chem. Soc.* **1954**, 3302−3313.
(46) Jeffrey, G. A.; McMullan, R. K.; Sax, M. *J. Am. Chem. Soc.* **1964**, *86*, 949−950.
(47) Sakurai, K. *J. Phys. Soc. Jpn.* **1961**, *16*, 1205−1213.
(48) Addadi, L.; Mil, J. v.; Lahav, M. *J. Am. Chem. Soc.* **1982**, *104*, 3422−3429.
(49) Evans, S.; Garcia-Garibay, M.; Omkaram, N.; Scheffer, J. R.; Trotter, J.; Wireko, F. *J. Am. Chem. Soc.* **1986**, *108*, 5648−5650.
(50) McBride, J. M.; Carter, R. L. *Angew. Chem., Int. Ed. Engl.* **1991**, *30*, 293−295.
(51) Sheldrick, G. M. *Acta Crystallogr.* **1990**, *A46*, 467.
(52) Sheldrick, G. M. SHELXL-93: Program for Crystal Structure Refinement, University of Göttingen, 1993.